$p27^{kip1}$ controls H-Ras/MAPK activation and cell cycle entry via modulation of MT stability

Linda Fabris[a,1], Stefania Berton[a,1], Ilenia Pellizzari[a,1], Ilenia Segatto[a], Sara D'Andrea[a], Joshua Armenia[a], Riccardo Bomben[b], Monica Schiappacassi[a], Valter Gattei[b], Mark R. Philips[c], Andrea Vecchione[d], Barbara Belletti[a,2], and Gustavo Baldassarre[a,2]

[a]Division of Experimental Oncology 2, Department of Translational Research, Centro di Riferimento Oncologico (CRO Aviano), National Cancer Institute, 33081 Aviano, Italy; [b]Clinical and Experimental Onco-Hematology Unit, Department of Translational Research, Centro di Riferimento Oncologico (CRO Aviano), National Cancer Institute, 33081 Aviano, Italy; [c]Perlmutter Cancer Institute, New York University School of Medicine, New York, NY 10016; and [d]Division of Pathology, II University of Rome "La Sapienza," Santo Andrea Hospital, 00100 Rome, Italy

Edited by Melanie H. Cobb, University of Texas Southwestern Medical Center, Dallas, TX, and approved October 1, 2015 (received for review May 4, 2015)

The cyclin-dependent kinase (CDK) inhibitor $p27^{kip1}$ is a critical regulator of the G1/S-phase transition of the cell cycle and also regulates microtubule (MT) stability. This latter function is exerted by modulating the activity of stathmin, an MT-destabilizing protein, and by direct binding to MTs. We recently demonstrated that increased proliferation in $p27^{kip1}$-null mice is reverted by concomitant deletion of stathmin in $p27^{kip1}$/stathmin double-KO mice, suggesting that a CDK-independent function of $p27^{kip1}$ contributes to the control of cell proliferation. Whether the regulation of MT stability by $p27^{kip1}$ impinges on signaling pathway activation and contributes to the decision to enter the cell cycle is largely unknown. Here, we report that faster cell cycle entry of $p27^{kip1}$-null cells was impaired by the concomitant deletion of stathmin. Using gene expression profiling coupled with bioinformatic analyses, we show that $p27^{kip1}$ and stathmin conjunctly control activation of the MAPK pathway. From a molecular point of view, we observed that $p27^{kip1}$, by controlling MT stability, impinges on H-Ras trafficking and ubiquitination levels, eventually restraining its full activation. Our study identifies a regulatory axis controlling the G1/S-phase transition, relying on the regulation of MT stability by $p27^{kip1}$ and finely controlling the spatiotemporal activation of the Ras-MAPK signaling pathway.

$p27^{kip1}$ | stathmin | Ras | cell cycle | microtubules

In multicellular organisms, each cell responds to external stimuli by finely modulating, in time and space, the activation of intracellular signal transduction pathways (1). Microtubules (MTs) represent one of the preferential networks involved in the ordered propagation of this information within the cell. MTs are organized into a polarized array that defines cellular polarity and serves to directionally transmit extra- to intracellular signals, and vice versa (2). MT functions are strictly linked to MT stability and dynamics, which govern signaling compartmentalization; activation levels of signal transduction pathways; and, consequently, several cellular processes, including cell cycle progression (2, 3). In particular, passage through the restriction point represents the prototype of a cellular process in which ordered integration of external and internal stimuli is strictly required (4).

A prominent role in this integrated system of growth control has been ascribed to the Ras-MAPK pathway (5). Ras is a small guanosine triphosphatase (GTPase) that localizes to the membrane and requires recycling in the vesicle compartment to be fully activated (6, 7). Full activation of the Ras-MAPK pathway results in ERK1/2 nuclear translocation and expression of specific transcription factors, such as EGR-1, Jun-B, and c-Fos (8). The regulation of this pathway by MTs has been proposed, but the molecular mechanisms have never been elucidated (2).

The Ras-MAPK cascade directly signals on two key regulators of cell cycle entry, namely, cyclin D1 and $p27^{kip1}$ (9). Cyclin D1 is transcribed following Ras-MAPK pathway activation, and the aberration of this molecular event underlies Ras-driven carcinogenesis (9, 10). Phosphorylation of $p27^{kip1}$ (hereafter p27) on Ser-10, following Ras-MAPK pathway activation, impinges on its stability and subcellular localization, and has been proposed to play a central role in Ras-driven tumorigenesis (11, 12).

We have recently demonstrated that p27 and stathmin genetically interact in vivo and that this interaction impinges on cell proliferation, eventually leading to organ size determination (13). Interestingly, both p27 and its interacting partner stathmin are implicated in the regulation of MT stability, with p27 acting as an MT stabilizer and stathmin acting as an MT destabilizer (14–17).

Here, we investigated in vitro and in vivo the role of p27/stathmin interaction in cell proliferation. Our findings unveil a regulatory axis controlling the G1/S-phase transition in mammalian cells, relying on the regulation of MT stability by p27 and eventually modulating the spatiotemporal activation of the Ras-MAPK signaling pathway.

Results

Stathmin Is Necessary for the Hyperproliferative Phenotype of p27 Null Primary Fibroblasts. In vivo, the proliferation-related phenotypes of p27-null animals are partially reverted by concomitant KO of stathmin (13). To understand the molecular mechanisms underlying this reversion, we generated primary mouse embryonic fibroblasts (MEFs) from WT, p27KO, stathmin KO (StmKO),

Significance

Different functions have been ascribed to $p27^{kip1}$, originally identified as a universal cyclin-dependent kinase (CDK) inhibitor, fundamental for the control of cell proliferation and tumor progression. Yet, not all p27 functions can be explained by its ability to bind and inhibit CDKs. Here, we demonstrate that $p27^{kip1}$ controls cell cycle entry also through a CDK-independent function, by regulating microtubule stability. Following growth factor stimulation, $p27^{kip1}$ prevents full activation of H-Ras, acting on its subcellular compartmentalization, eventually restraining the activation of the MAPK pathway. Our work provides additional understanding of the mechanisms regulating the cell cycle and anticipates potential implications in diseases characterized by deregulated proliferation, such as cancer.

Author contributions: B.B. and G.B. designed research; L.F., S.B., I.P., I.S., S.D., J.A., and R.B. performed research; M.S., V.G., M.R.P., and A.V. contributed new reagents/analytic tools; L.F., S.B., I.P., I.S., B.B., and G.B. analyzed data; R.B. performed and analyzed the microarray data; and B.B. and G.B. wrote the paper.

The authors declare no conflict of interest.

This article is a PNAS Direct Submission.

Freely available online through the PNAS open access option.

Data deposition: The microarray data reported in this paper have been deposited in the Gene Expression Omnibus (GEO) database, www.ncbi.nlm.nih.gov/geo (accession no. GSE31533).

[1]L.F., S.B., and I.P. contributed equally to this work.

[2]To whom correspondence may be addressed. Email: bbelletti@cro.it or gbaldassarre@cro.it.

This article contains supporting information online at www.pnas.org/lookup/suppl/doi:10.1073/pnas.1508514112/-/DCSupplemental.

and p27KO-StmKO [hereafter called double-KO (DKO)] mice and studied their proliferative behavior in vitro. Growth curve analyses demonstrated that DKO MEFs grew at an intermediate rate between WT and p27-null cells (Fig. 1*A*). BrdU incorporation (Fig. 1*B*) and TUNEL assays (Fig. 1*C*) indicated that the differences between p27KO and DKO MEFs were due to increased proliferation, rather than decreased apoptosis. No differences were observed between WT and StmKO MEFs (Fig. 1 *A–C*), which, accordingly, increased their number twofold in 4 days of culture ($n = 5$; WT = 1.96 ± 0.18, StmKO = 1.86 ± 0.20) (Fig. 1*D*). In the same time, p27KO MEFs increased about fourfold and DKO MEFs displayed an intermediate phenotype, increasing 2.8-fold (Fig. 1*D*). The same differences were also observed when MEFs were generated from different genetic backgrounds (*SI Appendix*, Fig. S1*A*). Overexpression of stathmin in WT, but not in p27KO, 3T3 fibroblasts led to an increase of their proliferation (*SI Appendix*, Fig. S1*B*), supporting the possibility that stathmin actively participated in the control of cell proliferation in a p27-dependent manner.

p27 Controls Cyclin-Dependent Kinase 2 Activity in a Stathmin-Independent Manner. Based on these results, we focused on the study of cell cycle progression in WT, p27KO, and DKO MEFs. In exponentially growing conditions, p27-null cells displayed a slight increase in S-phase population, compared with both WT and DKO cells (*SI Appendix*, Fig. S1*C*, *Upper*). Nevertheless, all tested primary MEFs responded similarly to contact inhibition (*SI Appendix*, Fig. S1*C*, *Lower*; high confluence), as already reported (18), suggesting that the differences in cell proliferation were not due to different ability to exit from the cell cycle.

The increased proliferation rate observed in p27-null cells and mice has been largely ascribed to increased cyclin-dependent kinase 2 (CDK2) and CDK1 activity (18–20). Similar to what we recently observed in vivo (13), p27KO cells displayed higher CDK2-, cyclin A-, and cyclin B1-associated kinase activities with respect to WT, but not DKO, MEFs (*SI Appendix*, Fig. S1 *D* and *E*). However, DKO cells showed decreased CDK4 activity with respect to p27KO cells (*SI Appendix*, Fig. S1*D*). Although stathmin is a substrate for both CDK2 and CDK1 (15, 21, 22), increasing doses of recombinant stathmin did not have an impact on the kinase activity of either endogenous or recombinant protein complexes (*SI Appendix*, Fig. S2 *A* and *B*).

Overall, our data confirm that the higher CDK2 activity observed in p27-null cells is not sufficient to explain their increased proliferation rate, as also proposed by others (19, 20).

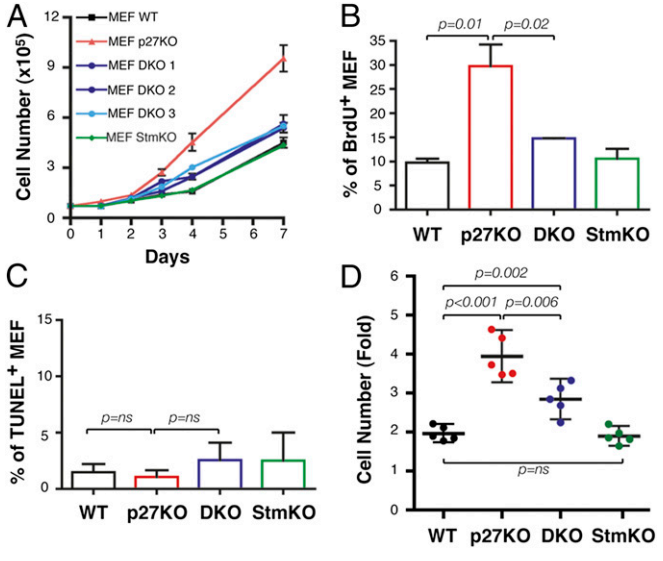

Fig. 1. Stathmin is necessary to sustain the proliferative phenotype of p27-null MEFs. (*A*) Growth curves of MEF WT, p27KO, DKO (three different embryos), and StmKO. Cells, plated on day 0, were counted at the indicated time points by a Trypan blue exclusion test. BrdU incorporation (*B*) and TUNEL (*C*) assays on exponentially growing MEF populations of the indicated genotypes were performed. The percentage of positive cells is indicated. (*D*) Duplication potential of MEF WT, p27KO, DKO, and StmKO cells, plated on day 0 and counted at day 4. The fold increase in cell number in five different MEF preparations/genotypes is reported. In each graph, statistical significance is calculated by the Student's *t* test and expressed by $P \leq 0.05$. ns, not significant.

p27/Stathmin Interaction Regulates Cell Cycle Entry. The above data suggested that G1/S-phase progression could be affected by stathmin loss in the absence of p27. Consistently, following serum stimulation, p27KO cells entered into S phase ∼4 h earlier than WT and DKO cells, showing an anticipated increase in cyclin A expression (S-phase marker) and CDK2, as well as cyclin E-, cyclin A-, and cyclin B1-associated kinase activities, with respect to both WT and DKO MEFs (*SI Appendix*, Fig. S1 *F–I*). Accordingly, overexpression of stathmin in WT fibroblasts resulted in a faster G1/S-phase transition, whereas stathmin knockdown in p27KO MEFs delayed cell cycle entry and cyclin A expression (*SI Appendix*, Fig. S3 *A–C*).

p27/Stathmin Interaction Regulates ERK1/2 Activity. To evaluate whether the different proliferative behavior was linked to alteration of specific pathways, we performed a microarray on MEFs of the genotypes of interest. By this approach, we identified a p27 signature comprising 263 genes differentially expressed between WT and p27KO cells and a DKO signature comprising the genes, among the 263, reverted in DKO fibroblasts ($n = 55$) (*SI Appendix*, Fig. S4). As a proof of principle, 15 differentially regulated genes were validated in quantitative RT-PCR analyses (*SI Appendix*, Fig. S4). Using the Gene Annotation Tool to Help Explain Relationships (GATHER) resource (gather.genome.duke.edu) and the Pathway-Express resource, linked to the Kyoto Encyclopedia of Genes and Genomes (KEGG) database (vortex.cs.wayne.edu/projects.htm), we identified the MAPK and mammalian target of rapamycin (mTOR) signaling pathways as significantly altered by p27 loss (*SI Appendix*, Tables S1 and S2).

Experimental testing of the bioinformatic results confirmed that activation of ERK1/2 was increased in p27KO with respect to both WT and DKO cells, whereas the mTOR pathway (using pAKT, pp70S6K, and pS6 as readouts) was not differentially activated (Fig. 2*A*). These observations were recapitulated in time course analyses (*SI Appendix*, Fig. S5*A*) and using different external stimuli, such as stimulation with EGF or IGF-1 (*SI Appendix*, Fig. S5*B*) or adhesion to ECM components (*SI Appendix*, Fig. S5*C*). Activation of the ERK1/2 seemed to be specifically controlled by p27/stathmin interaction, because it was decreased by reintroduction of $p27^{WT}$ in p27-null cells (Fig. 2*B*) and increased by reintroducing stathmin in DKO cells (Fig. 2*C*). Increased activation of ERK1/2 in p27-null cells was followed by increased expression of MAPK pathway nuclear targets, Egr-1 and Jun-B, both in p27KO MEFs and 3T3 fibroblasts (Fig. 2 *D* and *E* and *SI Appendix*, Fig. S5*D*). These observations were recapitulated in vivo, because both Jun-B and Egr-1 expression levels were significantly higher in thymus and spleen from p27KO mice than in respective organs from both WT and DKO mice (*SI Appendix*, Fig. S5*E*). Taken together, our data indicated that the MAPK pathway was consistently and robustly up-regulated in the absence of p27 and that this phenotype was reverted by loss of stathmin, both in vitro and in vivo.

p27 Regulates Activation of the MAPK Pathway in a CDK-Independent Manner. It is well known that p27 exerts CDK-dependent and -independent functions (14, 23). To understand whether lack of inhibition of CDKs could be responsible for the higher activity of ERK1/2 observed in p27-null cells, we treated p27KO MEFs with roscovitine, a chemical inhibitor of CDK activity. Roscovitine, used at a concentration able to inhibit CDK2 activity and S-phase entry of p27KO cells, did not modify pERK levels in p27KO cells (Fig. 3*A* and *SI Appendix*, Fig. S6 *A–C*) or the transcriptional

CELL BIOLOGY

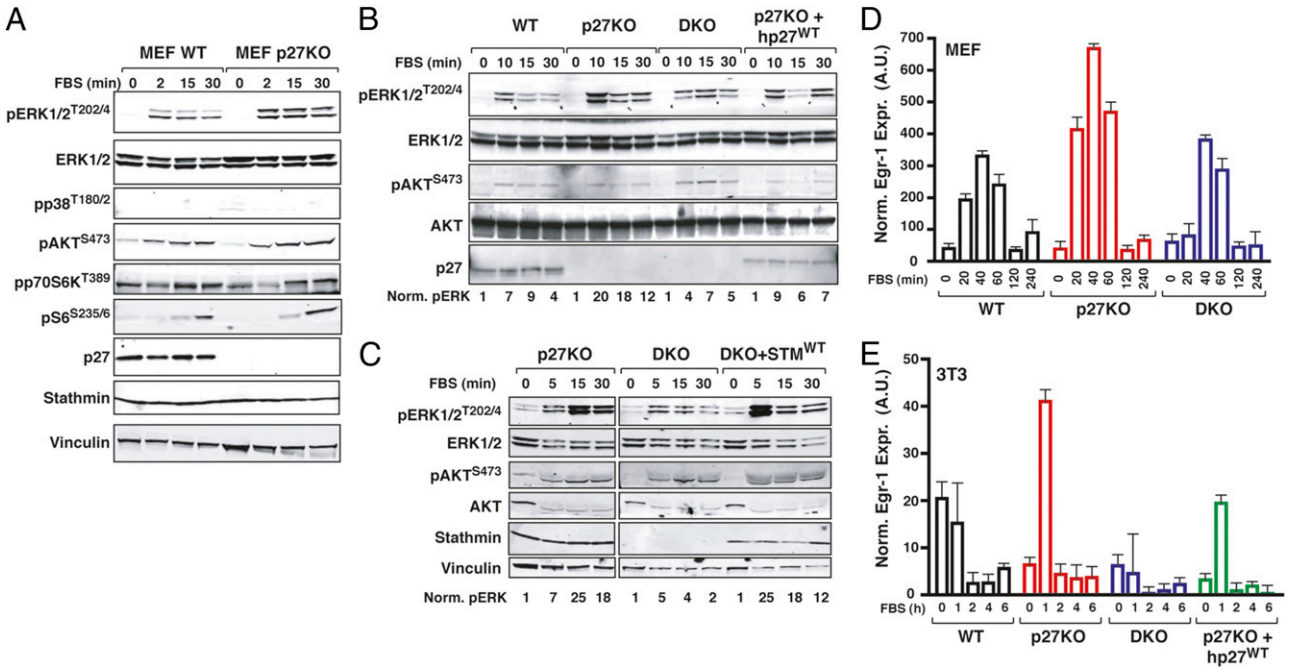

Fig. 2. Interaction of p27/stathmin regulates MAPK pathway activation. (*A*) Western blot analysis of the mTOR and MAPK pathway activation in WT and p27KO MEFs that were serum-starved and then stimulated with 10% serum (FBS) for the indicated times. Western blot analysis of pERK1/2 and pAKT in 3T3 fibroblasts of the indicated genotypes and 3T3 p27KO stably reexpressing p27 (*B*) or 3T3 DKO stably reexpressing stathmin (*C*) was performed. Cells were serum-starved and then stimulated with FBS for the indicated times. Numbers at the bottom of the panels indicate the quantification of normalized (Norm.) ERK1/2 phosphorylation levels. Quantitative RT-PCR analysis of Egr-1 in MEFs (*D*) or 3T3 fibroblasts (*E*) that were serum starved and then stimulated with 10% serum (FBS) for the indicated times. A.U., arbitrary units.

activation of the MAPK pathway target genes Egr-1, Jun-B, and c-Fos (Fig. 3*B* and *SI Appendix*, Fig. S6 *D* and *E*). Conversely, both events were strongly blocked by using a MEK1/2 inhibitor, U0126 (Fig. 3 *A* and *B* and *SI Appendix*, Fig. S6 *D* and *E*). Next, we transfected p27KO fibroblasts with the $p27^{CK-}$ mutant, which is unable to bind and inhibit the cyclin/CDK complexes, or with the $p27^{KR}$ mutant, which is prevalently localized in the cytoplasm (24). Both mutants exerted effects similar to the effects of the $p27^{WT}$ protein (Fig. 3*C* and *SI Appendix*, Fig. S6 *F* and *G*), indicating that MAPK pathway regulation is a cytoplasmic and CDK-independent function of p27.

Hyperactivation of the MAPK Pathway Is Responsible for the Faster Cell Cycle Entry of p27KO Cells. Sustained pERK levels and Egr-1 expression are critical events for cell cycle entry (5, 9). In line with these notions, we observed that inhibition of MAPK signaling, using the U0126 inhibitor, prevented the faster cell cycle entry of p27KO MEFs (Fig. 4*A*).

The MAPK pathway controls the G1/S transition by inducing cyclin D1 transcription and by delocalizing and favoring p27 degradation (9, 14), suggesting that in p27 null cells, the increased MAPK signaling would primarily have an impact on cyclin D1 expression. We tested this hypothesis by evaluating levels of cyclin D1 mRNA and protein in cells starved and then serum-stimulated. Our results showed that cyclin D1 levels increased 2 h earlier in p27KO cells compared with WT and DKO cells *SI Appendix*, Fig. S6 *H* and *I*). This effect was specifically dependent on MAPK activation, because it was reverted by the use of U0126 (*SI Appendix*, Fig. S6*H*). In line with these results, use of a specific inhibitor of CDK4/6 activity (PD0332991) (Fig. 4*A*) or silencing of cyclin D1 (Fig. 4*B*) resulted in delayed S-phase entrance of p27KO cells. Overall, these data suggested that p27 regulates the G1/S transition, at least in part, via the activation of the MAPK pathway in a stathmin-dependent manner.

MT-Dependent Transport Is Required for the Higher ERK1/2 Activation Observed in p27KO Cells. Endocytosis and endocytic trafficking are processes that rely on MTs and are strongly implicated in transmitting signals originating from the outside of the cell, and vice versa. Therefore, we tested whether p27/stathmin interaction could regulate MAPK pathway activation acting on these processes. To this aim, WT, p27KO, and DKO MEFs were stimulated with serum

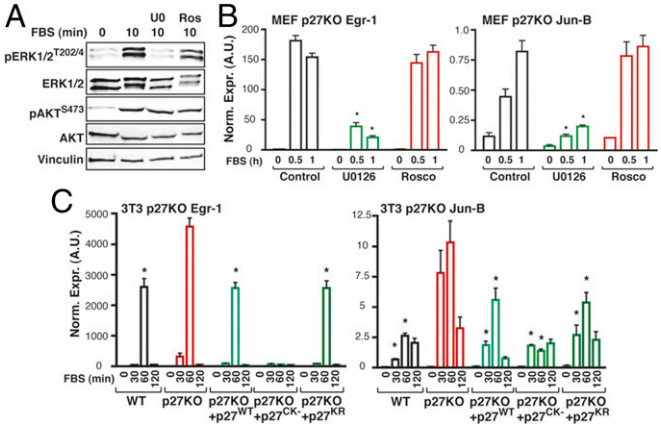

Fig. 3. p27 controls MAPK activation in a CDK-independent manner. (*A*) Western blot analysis of pERK1/2 and pAKT expression in MEF p27KO cells that were serum starved and then stimulated with 10% serum (FBS) for the indicated times, in the presence or absence of the MEK1 inhibitor U0126 (U0) or the pan-CDK inhibitor roscovitine (Ros, Rosco), as indicated. (*B*) Quantitative RT-PCR (qRT-PCR) analysis of Egr-1 and Jun-B in p27KO MEFs treated as described in *A*. $*P \leq 0.007$. (*C*) qRT-PCR analysis of Egr-1 and Jun-B in 3T3 fibroblasts of the indicated genotypes and in 3T3 p27KO cells stably expressing $p27^{WT}$, $p27^{CK-}$, or $p27^{KR}$. Cells were serum-starved and then stimulated with 10% serum (FBS) for the indicated times. $*P \leq 0.04$.

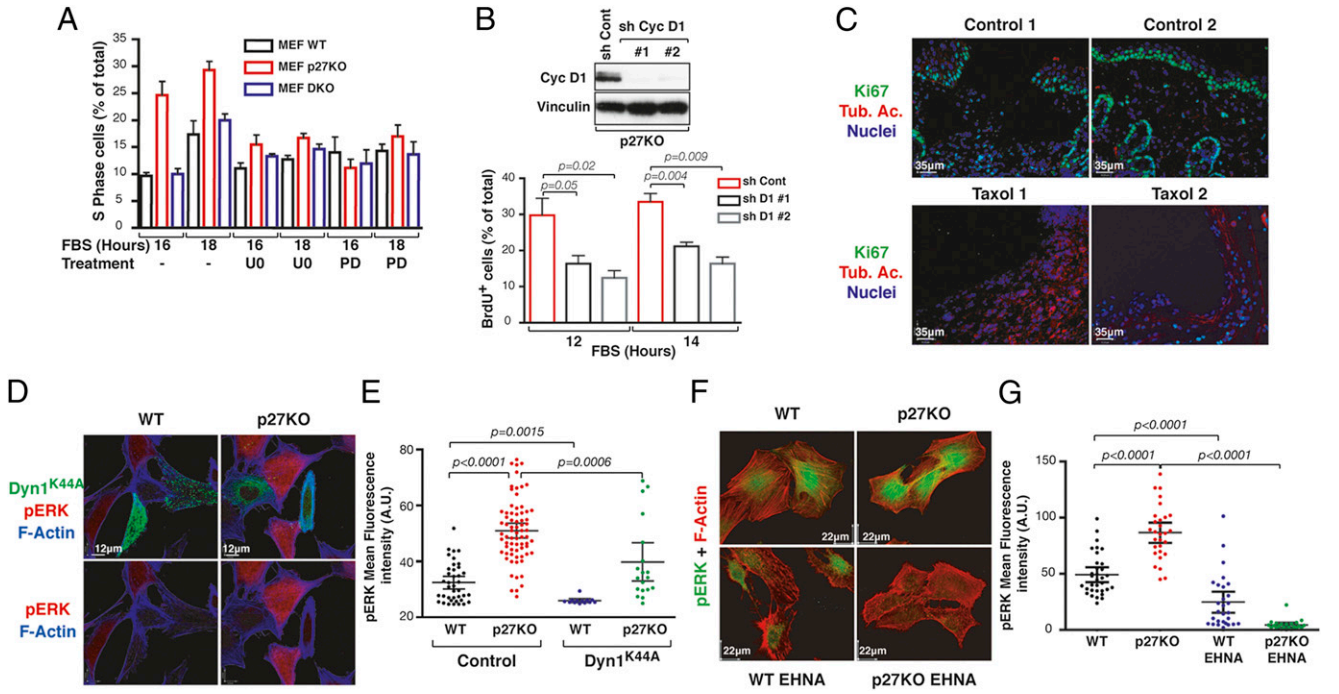

Fig. 4. Relative p27/stathmin expression levels control cell cycle progression via MT-dependent vesicle transport. (*A*) Percentage of S-phase in MEFs serum-starved and stimulated with 10% FBS, with or without U0126 (U0) or PD0332991 (PD), for the indicated times. (*B*) Percentage of BrdU incorporation of 3T3 p27KO, silenced for cyclin D1 expression, serum-starved and then stimulated with 10% FBS for the indicated times. The probability value was calculated by the Student's *t* test. (*Upper*) Cyclin (Cyc) D1 expression in control (sh Cont) and silenced (sh Cyc D1) cells is reported. Vinculin was used as a loading control. sh, short hairpin RNA. (*C*) Immunofluorescence analyses of Ki67 (green) and acetylated tubulin (Tub. Ac., red) in excisional wounds of the skin from p27KO mice treated with vehicle (control) or taxol (5 mg/kg). Typical images from two different mice per group are shown. Nuclei are stained with propidium iodide (pseudocolored in blue). (*D*) Immunofluorescence analyses of pERK1/2 (red) and F-actin (blue) in WT and p27KO fibroblasts, transfected with EGFP-dynamin1^{K44A} (Dyn^{K44A}) mutant (green) and stimulated with 10% serum (FBS) for 15 min. (*E*) Graph reports the quantification of pERK1/2 staining shown in *D*. (*F*) Immunofluorescence analyses of pERK1/2 (green) and F-actin (red) in WT and p27KO fibroblasts, treated or not with *erythro*-9-(2-Hydroxy-3-nonyl)adenine (EHNA) hydrochloride and then stimulated with serum for 5 min. (*G*) Graph reports the quantification of pERK1/2 staining shown in *F*. In *E* and *G*, each dot in the graph corresponds to one analyzed cell. Significant differences were calculated using the Mann–Whitney unpaired *t* test.

in the presence or absence of dynasore, which inhibits dynamin activity and prevents endocytosis (25), or low doses of taxol, an MT-stabilizing drug. Both compounds significantly decreased the extent of ERK1/2 phosphorylation (*SI Appendix*, Fig. S7*A*) and the transcription of its downstream targets Egr-1, c-Fos, and Jun-B (*SI Appendix*, Fig. S7 *B–D*). Accordingly, treatment with dynasore completely prevented cell cycle entry in serum-stimulated MEFs and 3T3 fibroblasts (*SI Appendix*, Fig. S7 *E* and *F*).

A skin wound-healing assay represents a paradigm for growth factor-induced spatiotemporal regulation of cell cycle entry in vivo, and it is associated with stathmin up-regulation (26) and p27 down-regulation (27). We performed this assay in p27KO mice, treating them or not with taxol for 48 h ($n = 4$ per group), to evaluate whether induction of MT stabilization in the p27KO context was accompanied by a decrease in cell cycle entry. As expected, taxol-treated mice displayed increased MT stabilization in cells facing the wound, as evaluated by the levels of acetylated tubulin (Fig. 4*C*, red). Interestingly, this MT stabilization was accompanied by a decrease of cell proliferation, as assessed by Ki67 staining (Fig. 4*C*, green).

To evaluate whether vesicle internalization and/or transport was altered by loss of p27, we used different approaches. First, we transfected WT and p27KO cells with dynamin1^{K44A}, a dynamin mutant that exerts a dominant negative effect on endocytosis (28). Overexpression of dynamin1^{K44A} significantly inhibited ERK activation in both WT and p27KO cells (Fig. 4 *D* and *E*), leaving the relative difference between the two cell types intact. On the contrary, impairment of vesicle transport by temperature shifting from 37 °C to 18 °C or 4 °C (6) prevented hyperactivation of MAPK in p27KO cells (*SI Appendix*, Fig. S8*A*), abolishing the difference between WT, p27KO, and DKO cells.

Vesicles and other intracellular cargos are transported along the MTs by kinesin- and dynein-motor proteins (29). Blocking this transport using a dynein inhibitor, *erythro*-9-(2-Hydroxy-3-nonyl)adenine (EHNA) hydrochloride (30), abolished serum-induced ERK phosphorylation in p27KO cells and strongly reduced it in WT cells, further indicating that p27KO cells were particularly sensitive to impairment of MT-dependent transport for signaling (Fig. 4 *F* and *G* and see *SI Appendix*, Fig. S8*B*).

p27 Inhibits H-Ras Activation via Stathmin. Data collected so far failed to identify a specific external stimulus able to hyperactivate the MAPK cascade in p27KO cells, suggesting that an intracellular upstream activator should be involved. The canonical upstream activator of the MAPK pathway is H-Ras, a small GTPase that localizes to the membrane (6) and requires recycling in the vesicle compartment to be fully activated (7). We thus investigated if H-Ras activity and localization were differentially regulated in WT, p27KO, and DKO cells. Serum stimulation induced a marked GFP–H-Ras membrane localization in p27KO cells, with respect to WT and DKO cells (Fig. 5*A* and *SI Appendix*, Fig. S9*A*). This observation was confirmed by confocal microscopy showing increased plasma membrane localization (*SI Appendix*, Fig. S9*A*) and a decreased amount of GFP–H-Ras in Rab-5–positive vesicles in p27KO cells, compared with WT or DKO cells (Fig. 5*B*). Rab-5 is a small GTPase regulator of vesicular trafficking, and it is involved in the mono- or biubiquitination of H-Ras (31), a process resulting in decreased H-Ras activity (31, 32). We thus tested whether H-Ras was differently mono- or biubiquitinated in the presence/absence of p27 and stathmin. Expression of p27 increased levels of H-Ras ubiquitination (Fig. 5 *C* and *D* and *SI Appendix*, Fig. S9 *B* and *C*), and coexpression of stathmin almost

completely reverted this effect (Fig. 5 *C* and *D* and *SI Appendix*, Fig. S9 *B* and *C*).

To verify if H-Ras ubiquitination levels were specifically modulated by p27/stathmin interaction, we used the $p27^{1–170}$ deletion mutant, which lacks the last 28 amino acids and is unable to bind and restrain stathmin activity (16, 33). Expression of $p27^{1–170}$ elicited no effect on H-Ras ubiquitination (*SI Appendix*, Fig. S9*C*). Consistently, endogenous H-Ras was less ubiquitinated in p27KO MEFs than in WT and DKO MEFs (*SI Appendix*, Fig. S9 *D* and *E*). In accord with the inhibitory role of ubiquitination on H-Ras activity, we also observed increased activity of endogenous H-Ras in p27KO MEFs (Fig. 5*E*) and mouse brains (*SI Appendix*, Fig. S9*F*), compared with both WT and DKO counterparts.

To get some insights on how stathmin could participate in the regulation of H-Ras activation, we investigated the localization of stathmin following serum stimulation in WT and p27KO MEFs. Serum stimulation induced a rapid membrane localization of stathmin only in p27KO cells (*SI Appendix*, Fig. S10 *A* and *B*). This localization was prevented by a temperature shift to 4 °C, indicating that it represented an active process occurring in p27KO cells (*SI Appendix*, Fig. S10 *A* and *B*, *Right*). Presence of stathmin at the plasma membrane in p27KO cells was accompanied by a strong decrease in the cellular pool of stable acetylated MTs, with respect to what was observed in WT cells (*SI Appendix*, Fig. S10 *C* and *D*).

These data indicated that p27, via MT stabilization, regulated H-Ras intracellular transport, eventually modulating its ubiquitination and activity. However, we could not exclude the possibility that p27 acted in a more general fashion, reducing the overall endocytic process. To approach this possibility, we verified whether p27 affected the internalization of fluorophore-conjugated transferrin and EGF, two commonly used markers of endosomal trafficking. Overexpression of either $p27^{WT}$ or $p27^{1–170}$ had no effect on the rate of EGF internalization (*SI Appendix*, Fig. S11 *A–C*). Similarly, absence of p27 did not change the internalization of transferrin by 3T3 fibroblasts (*SI Appendix*, Fig. S11 *D–F*). These data suggested that p27/stathmin interaction principally affected vesicle transport, rather than internalization.

Altogether, our data demonstrate that loss of p27, by releasing stathmin activity, alters H-Ras trafficking, diminishes its mono- or biubiquitination, and results in hyperactivation of MAPK signaling, which eventually contributes to anticipation of cell cycle entry.

Discussion

Signal transduction pathways need to be finely tuned and integrated in time and space to ensure that cells proliferate only in the presence of appropriate extracellular and intracellular conditions (1). Our data demonstrate that, following growth factor stimulation, $p27^{kip1}$ prevents full activation of H-Ras, modulating its trafficking in an MT-dependent manner. This mechanism might represent a useful strategy for a cell to prevent inappropriate proliferation. The contribution of MTs in propagating intracellular signals is well characterized (2). However, whether MTs and MT-dependent transport have a role in the regulation of cell cycle entry has not been clarified. A gradient of MT stabilization, due also to localized stathmin activity, has been observed in migrating and mitotic cells, and has been proposed as one of the main mechanisms by which an organized flux of information is delivered within the cell (34). Our data indicate that a similar mechanism participates in the regulation of cell cycle entry and point to the spatial and temporal regulation of H-Ras activity as a key event governed by MT stability and MT-dependent transport. This finding is independently supported by data recently reported by others (35), demonstrating that p27, by regulating MT organization, contributes to control the trafficking of Rab5-containing vesicles.

The central role of Ras proteins in driving proliferation, in both normal and cancer cells, has been widely demonstrated (36). The relevance of the cyclin D1/CDK4/6 complex and p27 expression in Ras-induced proliferation is also well established (8–10). In

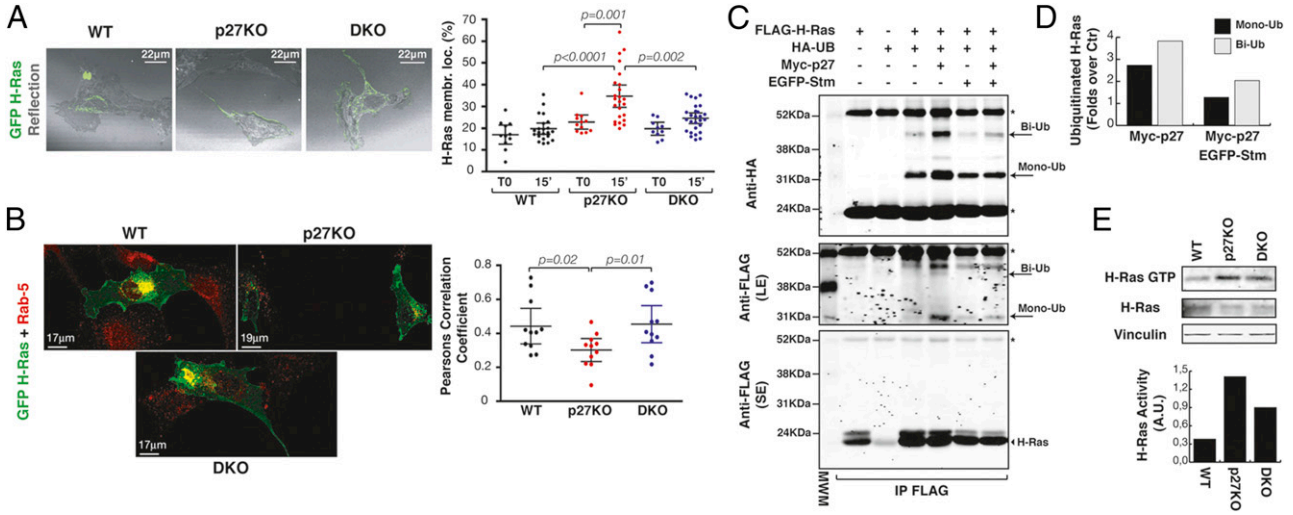

Fig. 5. Interaction of p27/stathmin controls H-Ras localization and activation. (*A*) Immunofluorescence analysis of H-Ras (GFP, green) superimposed on the reflection images of the same fields (gray, cell shape) in 3T3 WT, p27KO, and DKO fibroblasts that were serum-starved and stimulated with 10% serum (FBS) for 15 min at 37 °C. (*Right*) Graph reports the quantification of H-Ras membrane localization (membr. loc.), expressed as fluorescence intensity at the plasma membrane with respect to the total fluorescence of the cell. Each dot in the graph corresponds to one cell. Significant differences were calculated using the Mann–Whitney *t* test. (*B*) Immunofluorescence analysis of H-Ras (GFP, green) and Rab5 (red) expression in 3T3 WT, p27KO, and DKO fibroblasts. (*Right*) Graph reports the quantification of GFP–H-Ras in Rab-5–positive vesicles, expressed by the Pearson correlation coefficient. Significant differences were found using the Mann–Whitney *t* test. (*C*) Immunoprecipitation analysis of H-Ras mono- or biubiquitination in 293T/17 cells, transfected with FLAG-tagged H-Ras in the presence or absence of HA-tagged ubiquitin vector (HA-UB), Myc-tagged p27 vector, and EGFP-tagged stathmin vector, as indicated. Total cell lysates were immunoprecipitated with an anti-FLAG antibody and probed with anti-HA or anti-FLAG antibodies, as indicated. Arrows indicate mono- (Mono-Ub) and biubiquitinated (Bi-Ub) forms of H-Ras. Long exposure (LE) and short exposure (SE) of the same blot are shown. The arrowhead indicates unmodified FLAG-tagged H-Ras. Asterisks mark light and heavy IgG chains. (*D*) Graph reports the amount of mono- and biubiquitinated H-Ras, obtained by densitometric quantification of the blots in *C*, expressed as the fold increase of mono- or biubiquitination over the control (i.e., FLAG–H-Ras + HA-ubiquitin). Ctr, control. (*E*) Pull-down assays of active Ras (GTP-loaded Ras) in lysates from MEFs of the indicated genotypes. Vinculin was used as a loading control. H-Ras activity, normalized by H-Ras expression, is reported in the accompanying graph.

accord with our data, the study performed on CDK4/p27 DKO and CDK2/p27 DKO MEFs demonstrated that the faster entrance into S phase of p27-null MEFs could be prevented by genetic ablation of CDK4 (37), but not of CDK2 (19). Thus, our data, along with the current literature, suggest that p27 plays a double role in the control of cell proliferation by directly inhibiting CDK1 and CDK2 activity and by controlling the full activation of the Ras-MAPK-CDK4/6 pathway, via the regulation of MT stability.

We suggest here that the cell cycle machinery directly participates in the control of its upstream activator Ras-MAPK by simply delocalizing p27 in the cytoplasm upon growth factor stimulation. This mechanism could represent a fundamental checkpoint to prevent inappropriate proliferation, ensuring that a cell actually divides only when mitogenic stimuli are sufficient to overcome the threshold required to transit through the G1-S phase (5). Our data suggest that the expression of cytoplasmic p27 is involved in the control of this threshold. Similarly, it has been recently observed that the cyclin A2/CDK2 complex can activate AKT, directly participating in the control of its upstream activator (38).

The data presented here, conjunctly with the characterization of the p27/stathmin DKO mouse (13), suggest that this mechanism of control of cell cycle entry operates in multiple tissues, allowing for proper development of the entire organism. Most of the phenotypes of $p27^{kip1}$-null mice, linked to the hyperproliferative behavior of tissues and organs, were efficiently reverted by co-ablation of stathmin (13). On the contrary, StmKO mice did not display an overt proliferation-related phenotype (13, 39) and were as sensitive as WT animals to chemically induced tumorigenesis (39), suggesting that, in the presence of p27, other mechanisms can compensate for the effects of stathmin on cell proliferation.

Altogether, we delineate here a previously unknown mechanism involved in the control of cell cycle progression. Future research will clarify if this knowledge can be exploited to block uncontrolled proliferation in tumor cells, particularly in H-Ras–driven cancers.

Materials and Methods

Materials and methods are described in greater detail in *SI Appendix*.

Mice Models and Phenotypic Characterization. All animal procedures were approved by the Animal Care and Use Committee of the Centro di Riferimento Oncologico Aviano. C57BL/6 p27KO mice (The Jackson Laboratory) and C57BL/6 StmKO mice (39) were intercrossed to obtain p27 and stathmin DKO C57BL/6 mice. Mice have been thoroughly characterized by Berton et al. (13).

Cell Cultures. The primary WT, p27KO, StmKO, and p27/stathmin DKO MEFs were prepared from embryos at day 13.5, according to standard procedures, as described (16, 40, 41). The 3T3 fibroblasts were obtained from primary MEFs using the 3T3 immortalization protocol (16, 40, 41).

Proliferation, Apoptosis, and Ras Pull-Down Assays. Analyses of cell proliferation by growth curves, MTS assay (Promega), fluorescence-activated cell sorting analysis of DNA content, BrdU incorporation assay, Ki67 staining, and detection of apoptosis by TUNEL assay are techniques routinely performed in our laboratory (16, 24, 33, 39–41). Pull-down assays to evaluate H-Ras activity were performed using at least 3 mg of protein and GST-Raf (plasmid no. 13338; Addgene) (42).

ACKNOWLEDGMENTS. We thank Dr. Giorgio Scita, Dr. Milena Nicoloso, Dr. Alfonso Colombatti, and all members of our laboratory for helpful support, valuable suggestions, and critical reading of the manuscript. We thank Sara Benevol for expert technical assistance. This work was supported by Associazione Italiana Ricerca sul Cancro (AIRC) Grants IG 12854 (to G.B.) and IG 15902 (to B.B.) and by a Centro di Riferimento Oncologico Intramural Research Grant (to G.B.). S.B. is a recipient of an AIRC-Marie Curie Outgoing International Fellowship.

1. Scott JD, Pawson T (2009) Cell signaling in space and time: Where proteins come together and when they're apart. *Science* 326(5957):1220–1224.
2. Gundersen GG, Cook TA (1999) Microtubules and signal transduction. *Curr Opin Cell Biol* 11(1):81–94.
3. Janke C, Bulinski JC (2011) Post-translational regulation of the microtubule cytoskeleton: Mechanisms and functions. *Nat Rev Mol Cell Biol* 12(12):773–786.
4. Pardee AB (1974) A restriction point for control of normal animal cell proliferation. *Proc Natl Acad Sci USA* 71(4):1286–1290.
5. Zwang Y, et al. (2011) Two phases of mitogenic signaling unveil roles for p53 and EGR1 in elimination of inconsistent growth signals. *Mol Cell* 42(4):524–535.
6. Misaki R, et al. (2010) Palmitoylated Ras proteins traffic through recycling endosomes to the plasma membrane during exocytosis. *J Cell Biol* 191(1):23–29.
7. Abankwa D, Gorfe AA, Hancock JF (2007) Ras nanoclusters: Molecular structure and assembly. *Semin Cell Dev Biol* 18(5):599–607.
8. Rubinfeld H, Seger R (2005) The ERK cascade: A prototype of MAPK signaling. *Mol Biotechnol* 31(2):151–174.
9. Meloche S, Pouysségur J (2007) The ERK1/2 mitogen-activated protein kinase pathway as a master regulator of the G1- to S-phase transition. *Oncogene* 26(22):3227–3239.
10. Yu Q, Geng Y, Sicinski P (2001) Specific protection against breast cancers by cyclin D1 ablation. *Nature* 411(6841):1017–1021.
11. Jäkel H, Peschel I, Kunze C, Weinl C, Hengst L (2012) Regulation of p27 (Kip1) by mitogen-induced tyrosine phosphorylation. *Cell Cycle* 11(10):1910–1917.
12. Besson A, et al. (2006) A pathway in quiescent cells that controls p27Kip1 stability, subcellular localization, and tumor suppression. *Genes Dev* 20(1):47–64.
13. Berton S, et al. (2014) Genetic characterization of p27(kip1) and stathmin in controlling cell proliferation in vivo. *Cell Cycle* 13(19):3100–3111.
14. Belletti B, et al. (2005) p27(kip1) functional regulation in human cancer: A potential target for therapeutic designs. *Curr Med Chem* 12(14):1589–1605.
15. Belletti B, Baldassarre G (2011) Stathmin: A protein with many tasks. New biomarker and potential target in cancer. *Expert Opin Ther Targets* 15(11):1249–1266.
16. Baldassarre G, et al. (2005) p27(Kip1)-stathmin interaction influences sarcoma cell migration and invasion. *Cancer Cell* 7(1):51–63.
17. Godin JD, et al. (2012) p27(Kip1) is a microtubule-associated protein that promotes microtubule polymerization during neuron migration. *Dev Cell* 23(4):729–744.
18. Fero ML, et al. (1996) A syndrome of multiorgan hyperplasia with features of gigantism, tumorigenesis, and female sterility in p27(Kip1)-deficient mice. *Cell* 85(5):733–744.
19. Martín A, et al. (2005) Cdk2 is dispensable for cell cycle inhibition and tumor suppression mediated by p27(Kip1) and p21(Cip1). *Cancer Cell* 7(6):591–598.
20. Aleem E, Kiyokawa H, Kaldis P (2005) Cdc2-cyclin E complexes regulate the G1/S phase transition. *Nat Cell Biol* 7(8):831–836.
21. Brattsand G, Marklund U, Nylander K, Roos G, Gullberg M (1994) Cell-cycle-regulated phosphorylation of oncoprotein 18 on Ser16, Ser25 and Ser38. *Eur J Biochem* 220(2):359–368.
22. Andersen SS, et al. (1997) Mitotic chromatin regulates phosphorylation of Stathmin/Op18. *Nature* 389(6651):640–643.
23. Chu IM, Hengst L, Slingerland JM (2008) The Cdk inhibitor p27 in human cancer: prognostic potential and relevance to anticancer therapy. *Nat Rev Cancer* 8(4):253–267.
24. Armenia J, et al. (2014) Contact inhibition modulates intracellular levels of miR-223 in a p27kip1-dependent manner. *Oncotarget* 5(5):1185–1197.
25. Preta G, Cronin JG, Sheldon IM (2015) Dynasore - not just a dynamin inhibitor. *Cell Commun Signal* 13:24.
26. Schmitt S, et al. (2013) Stathmin regulates keratinocyte proliferation and migration during cutaneous regeneration. *PLoS One* 8(9):e75075.
27. Zhu X, Hu C, Zhang Y, Li L, Wang Z (2001) Expression of cyclin-dependent kinase inhibitors, p21cip1 and p27kip1, during wound healing in rats. *Wound Repair Regen* 9(3):205–212.
28. Lee E, De Camilli P (2002) Dynamin at actin tails. *Proc Natl Acad Sci USA* 99(1):161–166.
29. Hancock WO (2014) Bidirectional cargo transport: Moving beyond tug of war. *Nat Rev Mol Cell Biol* 15(9):615–628.
30. Beckerle MC, Porter KR (1982) Inhibitors of dynein activity block intracellular transport in erythrophores. *Nature* 295(5851):701–703.
31. Xu L, Lubkov V, Taylor LJ, Bar-Sagi D (2010) Feedback regulation of Ras signaling by Rabex-5-mediated ubiquitination. *Curr Biol* 20(15):1372–1377.
32. Yan H, Jahanshahi M, Horvath EA, Liu H-Y, Pfleger CM (2010) Rabex-5 ubiquitin ligase activity restricts Ras signaling to establish pathway homeostasis in Drosophila. *Curr Biol* 20(15):1378–1382.
33. Schiappacassi M, et al. (2008) p27Kip1 expression inhibits glioblastoma growth, invasion, and tumor-induced neoangiogenesis. *Mol Cancer Ther* 7(5):1164–1175.
34. Niethammer P, Bastiaens P, Karsenti E (2004) Stathmin-tubulin interaction gradients in motile and mitotic cells. *Science* 303(5665):1862–1866.
35. Nishimura YV, et al. (2014) Cdk5 and its substrates, Dcx and p27kip1, regulate cytoplasmic dilation formation and nuclear elongation in migrating neurons. *Development* 141(18):3540–3550.
36. Malumbres M, Barbacid M (2003) RAS oncogenes: The first 30 years. *Nat Rev Cancer* 3(6):459–465.
37. Tsutsui T, et al. (1999) Targeted disruption of CDK4 delays cell cycle entry with enhanced p27(Kip1) activity. *Mol Cell Biol* 19(10):7011–7019.
38. Liu P, et al. (2014) Cell-cycle-regulated activation of Akt kinase by phosphorylation at its carboxyl terminus. *Nature* 508(7497):541–545.
39. D'Andrea S, et al. (2012) Stathmin is dispensable for tumor onset in mice. *PLoS One* 7(9):e45561.
40. Berton S, et al. (2009) The tumor suppressor functions of p27(kip1) include control of the mesenchymal/amoeboid transition. *Mol Cell Biol* 29(18):5031–5045.
41. Belletti B, et al. (2010) p27kip1 controls cell morphology and motility by regulating microtubule-dependent lipid raft recycling. *Mol Cell Biol* 30(9):2229–2240.
42. Brtva TR, et al. (1995) Two distinct Raf domains mediate interaction with Ras. *J Biol Chem* 270(17):9809–9812.